J|A|C|S ARTICLES

Published on Web 11/04/2010

Tuning Electrochemical Rectification via Quantum Dot Assemblies

Gabriela P. Kissling, Christa Bünzli, and David J. Fermín*

School of Chemistry, University of Bristol, Cantock's Close, Bristol BS8 1TS, United Kingdom

Received July 12, 2010; E-mail: david.fermin@bristol.ac.uk

Abstract: A novel approach to tuning electrochemical rectification using 2D assemblies of quantum dots (QDs) is presented. Asymmetric enhancement of the oxidation and reduction currents in the presence of the $Fe(CN)_6^{3-/4-}$ redox couple is observed upon adsorption of QDs at thiol-modified Au electrodes. The extent of the electrochemical rectification is dependent on the average QD size. A molecular blocking layer is generated by self-assembling 11-mercaptoundecanoic acid (MUA) and an ultrathin film of poly(diallyldimethylammonium chloride) (PDADMAC) on the electrode. The polycationic film allows the electrostatic adsorption of 3-mercaptopropionic acid (MPA)-stabilized CdTe QDs, generating 2D assemblies with approximately 0.4% coverage. The QD adsorption activates a fast charge transfer across the blocking layer in which the reduction process is more strongly enhanced than the oxidation reaction. The partial electrochemical rectification is rationalized in terms of the relative position of the valence (VB) and conduction band (CB) edges with respect to the redox Fermi energy (ε_{redox}). Quantitative analysis of the exchange current density obtained from electrochemical impedance spectroscopy demonstrates that the enhancement of charge transport across the molecular barrier is strongly dependent on the position of the QD valence band edge relative to ε_{redox}. The average electron tunneling rate constant through the QD assemblies is estimated on the basis of the Gerischer model for electron transfer.

Introduction

Controlling charge transport across hybrid nanostructured systems incorporating metal nanoparticles, quantum dots, and carbon nanonostructures is a crucial aspect in developing functional sensing, optoelectronic, and photovoltaic devices.[1−4] Self-assembly of nanostructures is typically achieved by using functional molecular linkers, which exhibit specific chemical interactions with the substrates and nanostructures. Charge transfer across molecular linkers in electrochemical systems has been extensively studied as a function of their molecular structure.[5] For instance, it is well established that the distance dependence of electron transfer through self-assembled monolayers (SAMs) featuring alkyl groups is characterized by an exponential decay of the tunneling probability with a decay coefficient of $\beta \approx 0.8$ Å^{-1}.[5,6] However, there is growing evidence indicating that this behavior does not prevail in cases where metal nanostructures are present in the molecular bridges. Our group has shown that the electron transfer dynamics mediated by Au nanoparticles tethered to Au surfaces by carboxyl-terminated alkyl thiols are independent of the length of the alkyl chain up to distances as long as 10 Å.[7,8] Gooding and co-workers have also reported detailed studies based on Au nanoparticles[9,10] and carbon nanotubes[11] in which identical observations have been made. Ulstrup and co-workers have observed strong enhancement of electron transfer kinetics between redox proteins and electrodes mediated by Au nanoparticles.[12,13] The mechanism behind the apparent fast electron transport across insulating molecular layers mediated by metal nanostructures remains to be fully understood. In this contribution, we shall demonstrate that this process is strongly linked to the density of states (DOS) introduced by the nanostructures at the redox Fermi energy (ε_{redox}).

The rate of electron transport via molecular bridges can also be characterized by a strong dependence on the direction of the electron flow; a process commonly referred to as molecular rectification. Since the seminal work by Aviram and Ratner,[14] a large number of systems have been reported exhibiting molecular rectification.[15−18] Most of these systems feature

(1) Kamat, P. V. *J. Phys. Chem. C* **2008**, *112*, 18737.
(2) Katz, E.; Willner, I. *Angew. Chem., Int. Ed.* **2004**, *43*, 6042.
(3) Willner, I.; Willner, B. *Pure Appl. Chem.* **2002**, *74*, 1773.
(4) Love, J. C.; Estroff, L. A.; Kriebel, J. K.; Nuzzo, R. G.; Whitesides, G. M. *Chem. Rev.* **2005**, *105*, 1103.
(5) Adams, D. M.; et al. *J. Phys. Chem. B* **2003**, *107*, 6668.
(6) Newton, M. D.; Smalley, J. F. *Phys. Chem. Chem. Phys.* **2007**, *9*, 555.
(7) Zhao, J.; Bradbury, C. R.; Fermín, D. J. *J. Phys. Chem. C* **2008**, *112*, 6832.
(8) Bradbury, C. R.; Zhao, J.; Fermín, D. J. *J. Phys. Chem. C* **2008**, *112*, 10153.
(9) Le Saux, G.; Ciampi, S.; Gaus, K.; Gooding, J. J. *ACS Appl. Mater. Interfaces* **2009**, *1*, 2477.
(10) Shein, J. B.; Lai, L. M. H.; Eggers, P. K.; Paddon-Row, M. N.; Gooding, J. J. *Langmuir* **2009**, *25*, 11121.
(11) Chou, A.; Eggers, P. K.; Paddon-Row, M. N.; Gooding, J. J. *J. Phys. Chem. C* **2009**, *113*, 3203.
(12) Jensen, P. S.; Chi, Q.; Grumsen, F. B.; Abad, J. M.; Horsewell, A.; Schiffrin, D. J.; Ulstrup, J. *J. Phys. Chem. C* **2007**, *111*, 6124.
(13) Jensen, P. S.; Chi, Q.; Zhang, J. D.; Ulstrup, J. *J. Phys. Chem. C* **2009**, *113*, 13993.
(14) Aviram, A.; Ratner, M. A. *Chem. Phys. Lett.* **1974**, *29*, 277.
(15) Heath, J. R. *Annu. Rev. Mater. Sci.* **2009**, *39*, 1.
(16) McCreery, R. L.; Bergren, A. J. *Adv. Mater.* **2009**, *21*, 4303.
(17) Albrecht, T.; Guckian, A.; Ulstrup, J.; Vos, J. G. *Nano Lett.* **2005**, *5*, 1451.
(18) Chi, Q.; Zhang, J. D.; Ulstrup, J. *J. Phys. Chem. B* **2006**, *110*, 1102.

Scheme 1. Schematic Representation of the QD Array Generated via Layer-by-Layer Assembly[a]

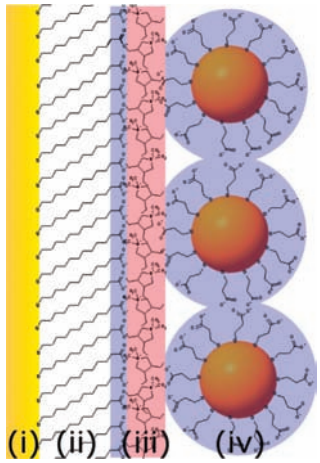

[a] Au electrodes (i) are sequentially modified by 11-mercaptoundecanoic acid (MUA) (ii), poly(diallyldimethylammonium chloride) (PDADMAC) (iii), and 3-mercaptopropionic acid (MPA)-stabilized CdTe QDs (iv). Scheme not drawn to scale.

donor−acceptor levels within the molecular bridges. Amplification of the electron transport rate takes place via resonant electron transfer occurring in the "forward bias" between the LUMO of the donor and the HOMO of the acceptor. Such resonant transport is hindered under "reverse bias". Whitesides and co-workers demonstrated that molecular rectification can also be observed with only a single redox center asymmetrically located in the molecular bridge.[19]

The present report describes a new class of electrochemical rectification mediated by 2D assemblies of quantum dots (QDs) at modified electrodes. The structure of the hybrid assembly is illustrated in Scheme 1. Our observations critically depend on a careful design of the molecular assembly and the electronic properties of the nanostructures. A self-assembled monolayer of 11-mercaptoundecanoic acid (MUA) offers a strong blocking layer to the direct electron transfer involving the $Fe(CN)_6^{3-/4-}$ couple. The adsorption of an ultrathin poly(diallyldimethylammonium chloride) (PDADMAC) film onto the carboxyl terminated SAM allows the electrostatic assembly of 3-mercaptopropionic acid (MPA) stabilized CdTe dots. This multistep approach ensures highly reproducible and controlled QD assemblies with regards to particle number density. The key novelty of this work is that by selecting different dot radii, the overlap between the DOS in the QD valence band and the Fermi energy of the redox species can be effectively varied. This parameter exhibits a profound effect not only on the symmetry of the current−voltage characteristics, but also on the rate of electron transfer. Furthermore, we employ the Gerischer formalism[20−23] to quantify the average tunneling rate constant associated with the QD-mediated process.

Experimental Section

CdTe Quantum Dot Synthesis and Assembly. The preparation of water-soluble CdTe QDs stabilized by 3-mercaptopropionic acid was performed on the basis of already established protocols (see Supporting Information).[24,25] Colloidal solutions of QDs with different sizes were stored in the dark. Prior to the assembly of QDs at the modified Au electrodes, the as-prepared particles were precipitated and redispersed in milli-Q water to remove excess reactants. QD assemblies were generated by electrostatic adsorption on freshly evaporated Au films modified by MUA and PDADMAC. The layer-by-layer assembly described in the Supporting Information generated randomly distributed 2D assemblies of QDs with a controlled particle number density. The exposed electrode surface area ($A = 0.071$ cm^2) was controlled using chemically inert adhesive PTFE tape (3M).

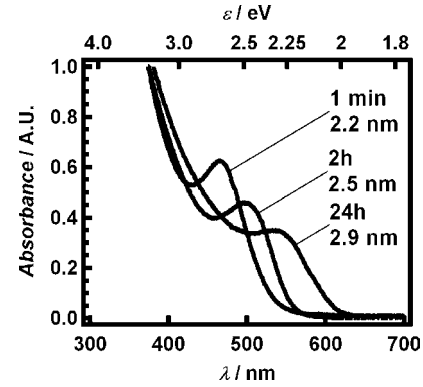

Figure 1. Absorption spectra of as-synthesized MPA-stabilized CdTe QDs. The average diameter was estimated from the exciton peak position employing eq 1.

AFM and Electrochemical Instrumentation. Topographic features associated with the electrostatic adsorption of the QDs on PDADMAC were monitored with acoustic AFM measurements (Molecular Imaging Pico LE). Cyclic voltammetry (CV) and electrochemical impedance spectroscopy (EIS) were performed with an Autolab PGSTAT 30 potentiostat in a standard three-electrode single compartment cell. A Pt wire and Ag/AgCl (3 M KCl) were used as secondary and reference electrodes, respectively. The electrolyte consisted of 1.0×10^{-3} mol dm^{-3} $K_4Fe(CN)_6$ and 1.0×10^{-3} mol dm^{-3} $K_3Fe(CN)_6$ in 0.1 mol dm^{-3} $NaClO_4$. The potential range scanned in CV was restricted to −0.1 and 0.5 V to avoid the anodic decomposition of the QDs.[24] EIS was measured at the formal redox potential (0.21 V vs Ag/AgCl) in the range of 130 mHz to 13 kHz, with an amplitude of 10 mV rms. Impedance spectra were recorded and analyzed using the Autolab FRA software. All electrochemical measurements were performed in a Faraday cage to minimize electrical noise and photoexcitation of the dots.

Results and Discussion

Two-Dimensional Assembly of CdTe QDs. Characteristic absorption spectra of the as-prepared CdTe colloidal solutions obtained after continuous reflux for 60 s, 2 h, and 24 h are exemplified in Figure 1. The exciton peak shifts toward higher wavelengths, indicating an increase in the average radius of the dots. As discussed previously, the growth rate is extremely slow due to the strong binding of the MPA groups to the dot surface.[24] The average dot diameter (d) can be estimated from the optical

(19) Chabinyc, M. L.; Chen, X. X.; Holmlin, R. E.; Jacobs, H.; Skulason, H.; Frisbie, C. D.; Mujica, V.; Ratner, M. A.; Rampi, M. A.; Whitesides, G. M. *J. Am. Chem. Soc.* **2002**, *124*, 11730.
(20) Gerischer, H. *Z. Physik. Chem. Neue Folge* **1960**, *26*, 223.
(21) Gerischer, H. *Z. Physik. Chem. Neue Folge* **1961**, *27*, 48.
(22) Sato, N. *Electrochemistry at Metal and Semiconductor Electrodes*; Elsevier Science: Amsterdam, 1998.
(23) Gerischer, H. In *Advances in Electrochemistry and Electrochemical Engineering*; Delahay, P., Ed.; Wiley Interscience: New York, 1961; Vol. 1, p 191.
(24) Kissling, G. P.; Fermín, D. J. *Phys. Chem. Chem. Phys.* **2009**, *11*, 10080.
(25) Zhang, H.; Yang, B. *Thin Solid Films* **2002**, *418*, 169.

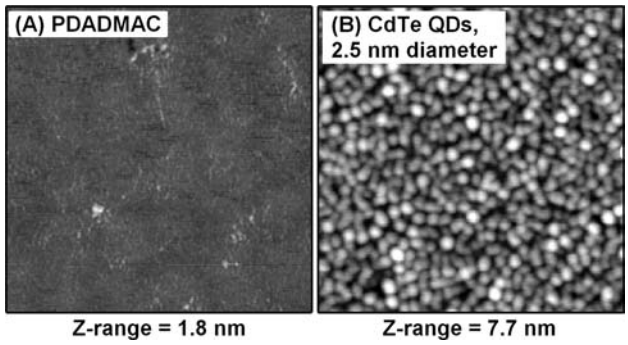

Figure 2. 1 μm × 1 μm topographic acoustic AFM images of the ultrathin PDADMAC layer (A) and a 2.5 nm diameter CdTe QD assembly (B).

band gap ($\varepsilon_{gap,OD}$) employing the relationship proposed by Sapra and Sarma on the basis of tight-binding calculations:[26]

$$\varepsilon_{gap,QD} = \varepsilon_{gap,bulk} + 5.77\exp(-d/8.45) + 1.33 \times \exp(-d/43.73) \quad (1)$$

where the band gap of bulk CdTe ($\varepsilon_{gap,bulk}$) is taken as 1.44 eV and d is expressed in ångströms. The results show that the average particle diameter changes from 2 to 3 nm during a 24 h growth period. High resolution TEM images confirmed that these estimations are consistent with the nanocrystal size (Supporting Information).

The electrostatic adsorption of CdTe colloids on a PDADMAC-modified surface generates a 2D layer with low density of aggregates as exemplified by the AFM images in Figure 2. The assembly was formed by electrostatic adsorption of an ultrathin PDADMAC layer on freshly cleaved mica, followed by 20 min exposure of the substrate to a 2.5 nm CdTe QD solution. The AFM image in Figure 2A corresponds to the PDADMAC-modified mica support. Topographic features of 70 − 80 pm are observed in distinctive parts of the surface. The image associated with the 2D assembly (Figure 2B) exhibits height fluctuations between 2 and 3 nm, which are consistent with the average diameter of the CdTe particles. Very few features with a height of 5 nm can be observed scattered around the surface, corresponding to dots adsorbed on top of other dots. Besides the presence of few dot clusters, the topography of the assembly is remarkably homogeneous. It should be mentioned that mica was chosen as a substrate to examine the fine details of the nanoparticle assembly. Our previous studies have shown that the distribution and particle number density of electrostatically adsorbed nanoparticles on ultrathin polyelectrolyte films are largely unaffected by the topography and chemical nature of the substrate.[27]

Analysis of the topographic features allowed estimation of the average dot number density, $\Gamma_{QD} = (7.6 \pm 1.0) \times 10^{10}$ cm^{-2}. Γ_{QD} is very much constant for the various QD particles sizes, which is expected in view of the narrow range of diameters investigated. On the basis of Γ_{QD} and the average cross-section of the dots, it can be estimated that the overall surface coverage is approximately 0.4%. This coverage appears somewhat lower than visually perceived from the AFM image in Figure 2B. The reason for this apparent discrepancy is the convolution of the tip shape featuring a 20 nm curvature radius with the QD topography. No tip shape correction was introduced to the AFM image; thus the QD cross-section appears artificially enlarged. Analysis of the phase image (not shown) also provides consistent values of Γ_{QD}. It should also be mentioned that small aggregates that cannot be resolved by the AFM tip may introduce a small margin of error to our surface coverage estimations.

Partial Electrochemical Rectification in the Presence of $Fe(CN)_6^{3-/4-}$. The evolution of the cyclic voltammograms associated with the sequential modification of the electrode surface is displayed in Figure 3. The $Fe(CN)_6^{3-/4-}$ couple exhibits a quasi-reversible behavior on the clean Au electrode (Figure 3A), showing a peak-to-peak separation of 66 mV at 5 mV s^{-1} and a formal redox potential of 0.21 V vs Ag/AgCl. These electrochemical responses are substantially attenuated in the presence of the MUA monolayer (Figure 3B). The inset in Figure 3B shows no peak currents and a current−potential relationship characteristic of electron transfer controlled kinetics at low overpotentials. The electrostatic adsorption of the PDADMAC film generated a slight increase in the Faradaic current at large overpotentials as exemplified in Figure 3C. The absence of peak current suggests that the blocking properties of the MUA layer are not significantly affected by the ultrathin polycationic film. As discussed in previous studies, the blocking properties of MUA are not only related to the well-ordered close-packed assembly of thiol molecules but also to the electrostatic repulsion between the ionized carboxyl termination and the negatively charged redox couple.[7,8,28] These electrostatic interactions are weakened by the adsorption of the polycation layer leading to an increase in the interfacial concentration of the $Fe(CN)_6^{3-/4-}$.

Figures 3D−F illustrate the effect of adsorbed QDs with diameters of 2.2, 2.5, and 2.9 nm, respectively, on the redox behavior of $Fe(CN)_6^{3-/4-}$. The electrochemical response is substantially enhanced upon adsorption of the dots, particularly in the reduction reaction. Two remarkable features can be observed when comparing the voltammograms in Figures 3D−F with those obtained for clean Au electrodes (Figure 3A): (i) the oxidation peak current is smaller than the reduction peak, and (ii) the oxidation peak current increases with increasing dot size. Slightly larger reduction current peaks with respect to the clean Au surface are also observed as a result of the strong affinity of the redox couple to the PDADMAC layer. Indeed, Luan et al. have recently shown that $Fe(CN)_6^{3-/4-}$ can be immobilized in QD-PDADMAC multilayer assemblies.[29] An increase in the surface concentration of the redox species manifests itself in an increase in the voltammetric peak currents as described by the Wopschall and Shain model.[30]

This unique electrochemical rectification can be rationalized in terms of the relative position of the band edges with respect to ε_{redox} as shown schematically in Figure 4. The dependence of the valence ($\varepsilon_{VB,QD}$/eV) and conduction band edges ($\varepsilon_{CB,QD}$/eV) on the dot diameter (d/Å) as a result of quantum confinement effects has been estimated by tight-binding model calculations, resulting in the following empirical functions:[26]

$$\varepsilon_{CB,QD} = \varepsilon_{CB,bulk} + \frac{16.38}{d^{0.92}} \quad (2)$$

(26) Sapra, S.; Sarma, D. D. *Phys. Rev. B* **2004**, *69*, 125304.
(27) Montes de Oca, M. G.; Fermín, D. J. *Electrochim. Acta*, **2010**, *55*, 8986.
(28) Zhao, J.; Bradbury, C. R.; Huclova, S.; Potapova, I.; Carrara, M.; Fermín, D. J. *J. Phys. Chem. B* **2005**, *109*, 22985.
(29) Luan, Q.; Li, J.; Yao, X. *Electroanalysis* **2009**, *21*, 1799.
(30) Wopschall, R.; Shain, I. *Anal. Chem.* **1967**, *39*, 1514.

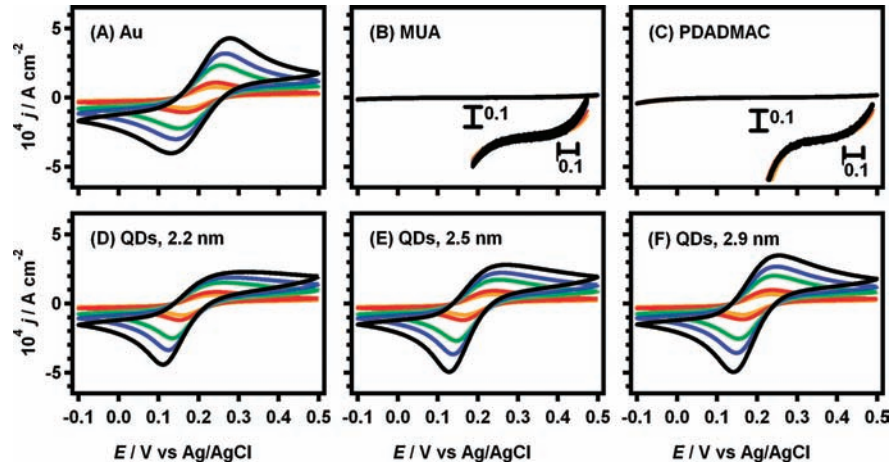

Figure 3. Cyclic voltammograms in the presence of 1.0×10^{-3} mol dm^{-3} $K_4Fe(CN)_6$ and $K_3Fe(CN)_6$ for a clean Au electrode (A) and after modification with MUA (B), MUA-PDADMAC (C) (insets representing 14× magnification), and MUA-PDADMAC-QDs of 2.2 (D), 2.5 (E), and 2.9 nm (F) diameter. Voltammograms were measured at 5, 10, 50, 100, and 200 mV s^{-1}.

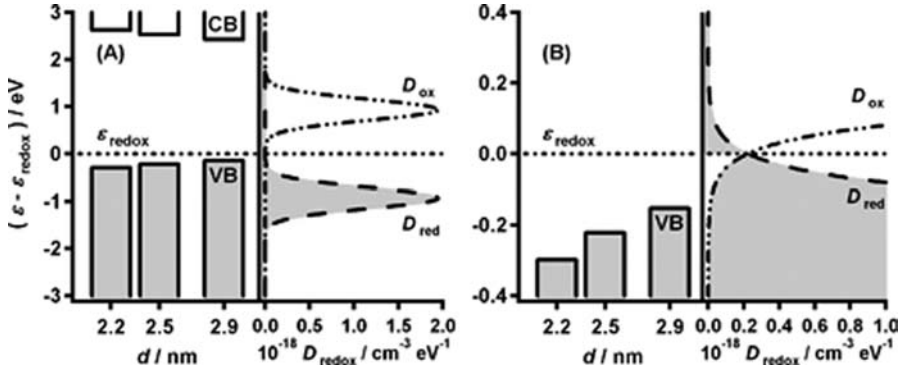

Figure 4. Energy diagram illustrating the relative position of the conduction and valence band edges with respect to D_{ox} and D_{red} (A). Expansion of the energy scale in the proximity of ε_{redox} (B).

$$\varepsilon_{VB,QD} = \varepsilon_{VB,bulk} + \frac{-19.03}{d^{1.13}} \quad (3)$$

where the valence and conduction band edges of bulk CdTe correspond to $\varepsilon_{CB,bulk} = 1.68$ eV and $\varepsilon_{VB,bulk} = 0.28$ eV vs ε_{redox} of $Fe(CN)_6^{3-/4-}$, respectively.[24] These values already take into account the surface dipole induced by the thiol layer, which shifts the band edges by 0.7 eV with respect to unmodified CdTe surfaces. The DOS associated with the oxidized (D_{ox}) and reduced (D_{red}) species can be expressed as[22]

$$D_{ox}(\varepsilon) = c_{ox}\frac{1}{\sqrt{4\lambda k_B T}}\exp\left(\frac{-(\varepsilon - \varepsilon_{ox})^2}{4\lambda k_B T}\right) \quad (4)$$

$$D_{red}(\varepsilon) = c_{red}\frac{1}{\sqrt{4\lambda k_B T}}\exp\left(\frac{-(\varepsilon - \varepsilon_{red})^2}{4\lambda k_B T}\right) \quad (5)$$

where c_{ox} and c_{red} are the bulk concentrations of the oxidized and reduced species, respectively. In this representation, the most probable energy levels of the oxidized (ε_{ox}) and reduced (ε_{red}) species are offset from ε_{redox} by the solvent reorganization energy ($\lambda = 90$ kJ mol^{-1} in the case of $Fe(CN)_6^{3-/4-}$).[31]

Gerischer's model describes the dynamics of interfacial electron transfer at semiconductor electrodes in terms of the overlap between the DOS at the semiconductor band edges with D_{ox} and D_{red}. The representation in Figure 4A shows that $\varepsilon_{CB,QD}$ is located more than 2.4 eV above ε_{redox} for all QD sizes, indicating that electron transfer mediated via the CB has a negligible contribution to the total Faradaic current. Consequently, the oxidation of $Fe(CN)_6^{4-}$ requires the generation of holes in the VB, while the reduction process will involve an isoenergetic electron transfer from $\varepsilon_{VB,QD}$ to the tail of D_{ox}. The extent of the mismatch between ε_{redox} and $\varepsilon_{VB,QD}$ for the various dot diameters is highlighted in Figure 4B. This diagram indicates a finite probability for the QD mediated reduction process when the Fermi level of the electrode is close to ε_{redox}. However, the oxidation reaction requires decreasing the electrode Fermi level (increasing the electrode potential) to promote the generation of holes in the valence band. This process manifests itself by a significant overpotential for the QD-mediated oxidation reaction.

Contrary to the case of bulk semiconductor electrodes, the origin of the electrochemical rectification is not related to the generation of a Schottky barrier at the solid|electrolyte interface. The small dimensions of the nanocrystals do not allow the formation of a depletion layer, and the band energies remain essentially flat across the QD structure. From this point of view, the QD-mediated electrochemical rectification can be compared to processes taking place at molecular assemblies. Closer examination of the voltammograms in Figure 3 shows that the

(31) Tsirlina, G. A.; Titova, N. V.; Nazmutdinov, R. R.; Petrii, O. A. *Russ. J. Electrochem.* **2001**, *37*, 15.

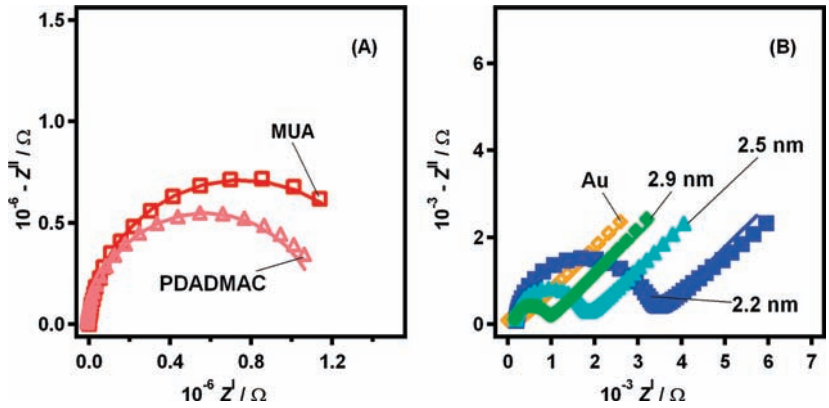

Figure 5. Complex representation of the impedance spectra (symbols) recorded at the formal redox potential and corresponding fits (lines) for the blocked Au electrodes (A) and after modification by QDs (B) with different diameters. For comparison, the impedance spectrum of an unmodified Au electrode is also included in (B).

extent of rectification depends not only on the dot size but also on the potential scan rate. The asymmetry in the anodic and cathodic current increases with increasing scan rate, indicating that this phenomenon is associated with a difference in the oxidation and reduction kinetics.

Average Exchange Current Density as a Function of the QD Size. Complex representations of the electrochemical impedance spectra at the formal redox potential for the various assemblies are illustrated in Figure 5. The spectra of MUA and MUA-PDADMAC modified electrodes (Figure 5A) are characterized by a semicircle with impedance values that are several orders of magnitude larger than what is obtained at clean Au surfaces (Figure 5B). The electrostatic assembly of PDADMAC generates a decrease in the impedance value. However, the dynamics remain essentially controlled by the kinetics of electron transfer across the modified surface. The trends observed in the impedance spectra are consistent with the voltammetric responses in Figure 3. Bode plots of the impedance spectra are included in the Supporting Information, further illustrating the effect of each modification step on the dynamic electrochemical responses.

The electrostatic adsorption of CdTe QDs at the MUA-PDADMAC modified electrode brings about a significant decrease in the magnitude of the impedance responses, as shown in Figure 5B. The time constant associated with the kinetics of electron transfer (frequency at the maximum of the semicircle) shifts to higher frequencies as the average dot radius increases. For all QD assemblies, impedance responses are higher than in the case of clean Au surfaces. The dynamic responses exemplified in Figure 5B provide further strong evidence of the size-dependent kinetics of QD-mediated electron transfer under the present experimental conditions.

The impedance responses associated with the various modification steps can be quantitatively analyzed employing the phenomenological Randles circuit (see Supporting Information). As discussed further below, the physical meaning of the phenomenological charge transfer resistance (R_{ct}) is determined by the transport mechanism across the modified surface. In addition to R_{ct}, the uncompensated resistance ($R_\Omega \approx 150\ \Omega$ on average for all electrodes), the interfacial capacitance (C_{int}), and the Warburg element (σ) were estimated from nonlinear least-square fits to the impedance spectra. The lines in Figure 5 illustrate typical fits obtained over the whole frequency range.

The parameters extracted from the analysis of the impedance spectra are summarized in Table 1. The values of R_{ct} are

Table 1. Charge Transfer Resistance (R_{ct}), Interfacial Capacitance (C_{int}), and Exchange Current Density (j_0) Estimated from Impedance Spectra

	R_{CT} / Ω	10^7 C_{int} / F	j_0 / A cm^{-2}
Au	$(2.5 \pm 0.2) \times 10^2$	7.3 ± 2.6	$(1.4 \pm 0.1) \times 10^{-3}$
MUA	$(9.5 \pm 4.1) \times 10^5$	3.7 ± 0.7	$(4.3 \pm 1.9) \times 10^{-7}$
PDADMAC	$(1.2 \pm 0.6) \times 10^5$	2.2 ± 0.2	$(3.9 \pm 2.7) \times 10^{-6}$
CdTe 2.2 nm	$(3.3 \pm 0.4) \times 10^3$	3.2 ± 1.2	$(1.1 \pm 0.1) \times 10^{-4}$
CdTe 2.5 nm	$(1.4 \pm 0.1) \times 10^3$	3.9 ± 2.3	$(2.5 \pm 0.2) \times 10^{-4}$
CdTe 2.9 nm	$(7.9 \pm 1.0) \times 10^2$	2.3 ± 0.3	$(4.6 \pm 0.5) \times 10^{-4}$

significantly affected by each electrode modification step, while C_{int} and σ only exhibit minor changes. The decrease in C_{int} upon adsorption of the MUA layer is consistent with the formation of a molecularly thin dielectric layer at the metal|electrolyte interface.[8] No significant changes are further observed upon adsorption of PDADMAC and QDs, confirming that the integrity of the self-assembled monolayer remains unaffected during the layer-by-layer assembly. The average value of $\sigma = (2.8 \pm 0.3) \times 10^3\ \Omega\ s^{-0.5}$ obtained for the QD assemblies was consistent with the diffusion coefficient of the redox couple in solution (see Supporting Information).

The blocking effect induced by the MUA manifests itself by an increase of 3 orders of magnitude in R_{ct}. The adsorption of PDADMAC brings about a decrease in R_{ct} as a result of the reversal in surface dipole induced by the polycationic film.[32] Despite the charge overcompensation, the electrochemical response remains essentially controlled by the dynamics of electron transfer across the underlying MUA monolayer. The significant decrease in R_{ct} upon adsorption of the QDs provides clear evidence of a change in the charge transfer mechanism. The dependence of R_{ct} on the average QD size further suggests that the electronic structure of the dots plays a role in the mediated charge transfer kinetics.

The phenomenological R_{ct} of the modified electrode involves two parallel paths for electron transfer represented by the charge transfer resistance across the blocking layer ($R_{ct,film}$) and the QD-mediated process ($R_{ct,QD}$). As discussed in more detail in the Supporting Information, $R_{ct,QD}$ comprises a series of sequential steps associated with (i) charge transfer from the redox couple to the QDs followed by (ii) charge transfer from the QDs to the electrode surface. Taking the former step as the main contributor to $R_{ct,QD}$, the observed R_{ct} can be approximated to[7]

(32) Carrara, M.; Kakkassery, J. J.; Abid, J.-P.; Fermín, D. J. *ChemPhysChem* **2004**, *5*, 571.

$$R_{ct} = \frac{R_{ct,QD}R_{ct,film}}{R_{ct,QD} + R_{ct,film}} \approx R_{ct,QD} \quad (6)$$

The data in Table 1 indicates that R_{ct} is essentially determined by the QD-mediated process, that is, $R_{ct,QD} \ll R_{ct,film}$. Consequently, the exchange current density ($j_{QD,0}$) associated with the electron transfer mediated by the QD assembly can be directly extracted from

$$R_{ct,QD} = \frac{RT}{nFj_{QD,0}A} \quad (7)$$

where A is the geometrical surface area of the electrode. The dependence of $j_{QD,0}$ on the average QD diameter is also shown in Table 1. This parameter fundamentally involves the contribution of each individual QD in the 2D assembly to the charge transfer dynamics at the formal redox potential.

The measured $j_{QD,0}$ contains contributions from partial exchange current densities developed at the valence ($j_{VB,0}$) and conduction band edges ($j_{CB,0}$) of the dots. The Gerischer model establishes that the current density is not only dependent on the corresponding tunneling rate constants but also on the overlap of the DOS of the semiconductor and the redox species. Considering that the maximum charge transfer effectively occurs within k_BT from the QD band edges,[21,23] these contributions can be expressed as:

$$j_{VB,0} = ek_pD_{red}(\varepsilon = \varepsilon_{VB,QD} - k_BT)N_{VB} \times \exp\left(\frac{-(\varepsilon_{redox} - \varepsilon_{VB,QD})}{k_BT}\right) \quad (8)$$

$$j_{CB,0} = ek_nD_{ox}(\varepsilon = \varepsilon_{CB,QD} + k_BT)N_{CB} \times \exp\left(\frac{-(\varepsilon_{CB,QD} - \varepsilon_{redox})}{k_BT}\right) \quad (9)$$

where k_p and k_n correspond to the electron tunneling rate constants at the valence and conduction band edges, respectively. The effective DOSs in the conduction and valence band involved in the charge transfer process are introduced in the terms N_{CB} and N_{VB}. The latter can be estimated from

$$N_{VB} = 2\left(\frac{m_em_h^*k_BT}{2\pi\hbar^2}\right)^{3/2} = 5.2 \times 10^{18}\ \text{cm}^{-3} \quad (10)$$

where m_e and m_h^* are the electron mass and the effective mass of holes (0.35 for CdTe) in the valence band. As mentioned previously, $\varepsilon_{CB,QD}$ is located more than 2.4 eV above ε_{redox} for all QD sizes, rendering the last term in eq 9 vanishingly small. Consequently, the contribution of $j_{CB,0}$ to the total exchange current density is negligible, that is, $j_{QD,0} \approx j_{VB,0}$.

The electron tunneling rate constant mediated by the valence band of the QDs can be estimated from eq 8, and the data in Table 1, resulting in an average $k_p = (2 \pm 1) \times 10^{-17}$ cm^4 s^{-1}. This result confirms that the dependence of the exchange current density on QD size arises from changes in the mismatch between $\varepsilon_{CB,QD}$ and ε_{redox} rather than from changes in k_p. We are not aware of any comparable analysis in the literature; however, it is important to put the estimated value of k_p in the context of the electron transfer theory at semiconductor electrodes. Lewis has investigated in detail the dynamics of electron transfer at semiconductor electrodes, suggesting that the maximum rate constant for electron transfer is of the order of 10^{-17}–10^{-16} cm^4 s^{-1}.[33,34] Smith et al. concluded that Lewis' assumption of approximating electrons in a semiconductor as hard spheres with a plane of closest approach to the interface underestimates the maximum k_p by several orders of magnitude.[35] Nozik and coworkers have reported outer-sphere electron transfer rate constants in the order of 10^{-12} cm^4 s^{-1} at passivated p-GaAs electrodes.[36] In the context of this work, it should be considered that we are dealing with an assembly of discrete dots rather than extended semiconductor surfaces. The particle number density in the 2D layer is $\Gamma_{QD} = (7.6 \pm 1.0) \times 10^{10}$ cm^{-2}; therefore, the average rate constant per dot can be estimated to be of the order of 5×10^{-15} cm^4 s^{-1}. It is clear that a more robust theoretical framework is required for further rationalization of the apparently fast electron transfer dynamics mediated by the CdTe dots. However, the k_p values estimated from this analysis are consistent with a mechanism in which the rate-determining step involves the charge transfer between the redox species and individual dots.

Conclusions

The present studies uncover fundamental aspects of the size-dependent electrochemical rectification associated with QD assemblies. The sequential modification of Au electrodes by MUA and PDADMAC generates a strong barrier for electron transfer in the presence of $Fe(CN)_6^{3-/4-}$. The adsorption of a submonolayer of MPA-stabilized CdTe dots induces an asymmetric enhancement of the electron transfer response, which can be rationalized in terms of the relative position of the valence and conduction band edges with respect to the redox Fermi energy. Considering that $\varepsilon_{CB,QD}$ is located more than 2.4 eV above ε_{redox}, the mediated charge transfer predominantly occurs via the valence band. As the average diameter of the dots decreases, $\varepsilon_{VB,QD}$ shifts further below ε_{redox}, thereby increasing the overpotential for the generation of holes required for the oxidation process. On the other hand, there is no observable size dependence in the reduction current due to a more effective overlap between D_{ox} and $\varepsilon_{VB,QD}$. These observations are consistent with the dependence of the formal charge transfer resistance on the average dot size as probed by impedance spectroscopy. The results clearly show that the phenomenological exchange current density increases with increasing dot size. The origin of this trend is associated with changes in the overlap between $\varepsilon_{VB,QD}$ and ε_{redox} rather than with the average tunneling rate constant. In other words, the QD assembly exhibits a more "metal-like" behavior with increasing dot size.

We have proposed that the long-range charge transfer mediated by metal nanoparticles involves a resonant transport activated by an increase in the DOS at the redox energy in the molecular assembly.[8] Indeed, metal nanostructures induce fast charge transfer through alkyl-based monolayers, while such effects are not observed in identical assemblies involving insulating nanostructures (SiO_2).[37] The results in this Article clearly show that systematic increment of the DOS in the vicinity of the redox Fermi energy translates into a progressive enhancement of electron transfer kinetics. These findings can have

(33) Fajardo, A. M.; Lewis, N. S. *Science* **1996**, *274*, 969.
(34) Lewis, N. S. *Annu. Rev. Phys. Chem.* **1991**, *42*, 543.
(35) Smith, B. B.; Halley, J. W.; Nozik, A. *J. Chem. Phys.* **1996**, *205*, 245.
(36) Rosenwaks, Y.; Thacker, B. R.; Ahrenkiel, R. K.; Nozik, A. J. *J. Phys. Chem.* **1992**, *96*, 10096.
(37) Zhao, J.; Wasem, M.; Bradbury, C. R.; Fermín, D. J. *J. Phys. Chem. C* **2008**, *112*, 7284.

important implications on the design of hybrid photovoltaic and optoelectronic devices featuring QD materials. We believe that QD assemblies can be used not only as light harvesting elements in excitonic solar cells, but also as mediators for the injection of hot carriers. In this sense, a demonstration of hot-carrier injection from QDs has recently been reported by Tisdale et al.[38]

Acknowledgment. We are indebted to the School of Chemistry of the University of Bristol, the Swiss National Science Foundation (PP0022--116898), as well as the EPSRC SUPERGEN Consortium on Excitonic Solar Cells for financial support. We also acknowledge the contributions of Laurence Asprey and Jonathan Jones.

Supporting Information Available: Detailed description of the QD synthesis and a representative high resolution TEM image of MPA-stabilized CdTe quantum dots obtained after 24 h synthesis. Methodology for assembling QDs, detailed analysis of the impedance spectra, and the complete list of authors for ref 5. This material is available free of charge via the Internet at http://pubs.acs.org.

JA106149G

(38) Tisdale, W. A.; Williams, K. J.; Timp, B. A.; Norris, D. J.; Aydil, E. S.; Zhu, X. Y. *Science* **2010**, *328*, 1543.